Mimic of the Green Fluorescent Protein β-Barrel: Photophysics and Dynamics of Confined Chromophores Defined by a Rigid Porous Scaffold

Derek E. Williams,[†] Ekaterina A. Dolgopolova,[†] Perry J. Pellechia,[†] Andrei Palukoshka,[†] Thomas J. Wilson,[†] Rui Tan,[†] Josef M. Maier,[†] Andrew B. Greytak,[†] Mark D. Smith,[†] Jeanette A. Krause,[‡] and Natalia B. Shustova*,[†]

[†]Department of Chemistry and Biochemistry, University of South Carolina, Columbia, South Carolina 29208, United States

[‡]Department of Chemistry, University of Cincinnati, Cincinnati, Ohio 45221, United States

ⓈSupporting Information

ABSTRACT: Chromophores with a benzylidene imidazolidinone core define the emission profile of commonly used biomarkers such as the green fluorescent protein (GFP) and its analogues. In this communication, artificially engineered porous scaffolds have been shown to mimic the protein β-barrel structure, maintaining green fluorescence response and conformational rigidity of GFP-like chromophores. In particular, we demonstrated that the emission maximum in our artificial scaffolds is similar to those observed in the spectra of the natural GFP-based systems. To correlate the fluorescence response with a structure and perform a comprehensive analysis of the prepared photoluminescent scaffolds, ^{13}C cross-polarization magic angle spinning solid-state (CP-MAS) NMR spectroscopy, powder and single-crystal X-ray diffraction, and time-resolved fluorescence spectroscopy were employed. Quadrupolar spin−echo solid-state ^{2}H NMR spectroscopy, in combination with theoretical calculations, was implemented to probe low-frequency vibrational dynamics of the confined chromophores, demonstrating conformational restrictions imposed on the coordinatively trapped chromophores. Because of possible tunability of the introduced scaffolds, these studies could foreshadow utilization of the presented approach toward directing a fluorescence response in artificial GFP mimics, modulating a protein microenvironment, and controlling nonradiative pathways through chromophore dynamics.

modes by β-barrel interactions makes fluorescence the main pathway for energy release.[6]

Herein, we demonstrate a novel approach to mimic the GFP β-barrel behavior toward chromophores with benzylidene imidazolinone cores by engineering an artificial porous multifunctional scaffold (Scheme 1). We tried to consolidate the

Scheme 1[a]
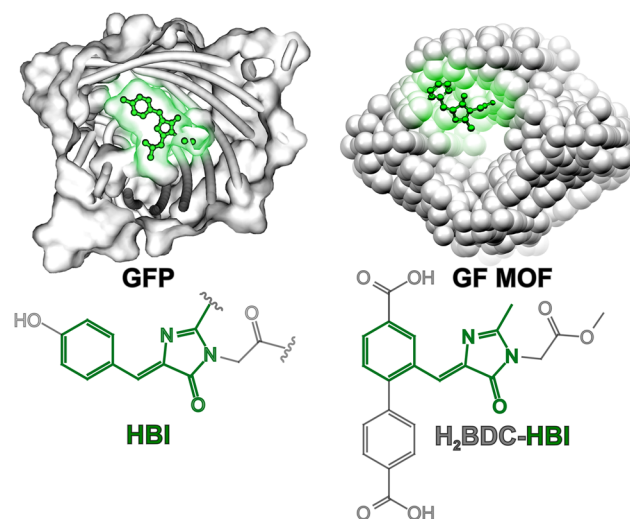
[a](left) GFP with the HBI chromophore structure emphasized. (right) A green fluorescent MOF (GF MOF) constructed from the HBI-based analogue, H₂BDC−HBI, using solvothermal synthesis or post-synthetic modification (PSM) procedures.

experience gained from previous studies of emission recovery in the molecular[8,10−13] and hybrid HBI-based systems,[14−17] which provided us with insight that modulation of the chromophore environment could be feasible in porous extended structures (e.g., metal−organic frameworks (MOFs)). Because of the tunability of framework structures,[18−25] we envisioned that the presented approach could be utilized to (i) study the chromophore structure−property relationship by directing its

R estriction of chromophore nonradiative pathways is an application-driven requirement to enhance material emission response.[1−5] In many cases, chromophore photophysical properties can be tuned as a function of its molecular conformation or environment. For instance, emission of 4-hydroxybenzylidene imidazolinone (HBI), the fluorophore responsible for photoluminescence of the commonly used biomarker GFP, is mainly defined by the chromophore−β-barrel interactions.[6] The unconfined chromophores with a benzylidene imidazolinone core are almost nonemissive,[7,8] which is in agreement with a rapid loss of fluorescence response observed in denatured GFP.[9] Remarkably, GFP refolding can restore protein emission, meaning that suppression of low-energy vibrational

fluorescence response through a scaffold design and therefore study almost nonemissive[7,8] synthetic HBI analogues, (ii) mimic the chromophore local environment in the GFP β-barrel by tuning the pore aperture and habitat, (iii) control chromophore molecular conformations through change of the scaffold size, and (iv) affect chromophore dynamics through structural transformations. As a model, we prepared a novel HBI-based chromophore (Scheme 1) and developed two ways to immobilize it inside the rigid scaffold. In addition to time-resolved photoluminescence measurements employed to study chromophore photophysical properties, we utilized a combination of solid-state quadrupolar echo ^{2}H NMR, ^{13}C CP-MAS NMR spectroscopic techniques, and theoretical calculations to probe the chromophore dynamics inside the engineered rigid scaffolds.

Scheme 2 illustrates two approaches, which were pursued to construct a porous mimic of the GFP β-barrel: (**I**) an HBI-based

Scheme 2[a]
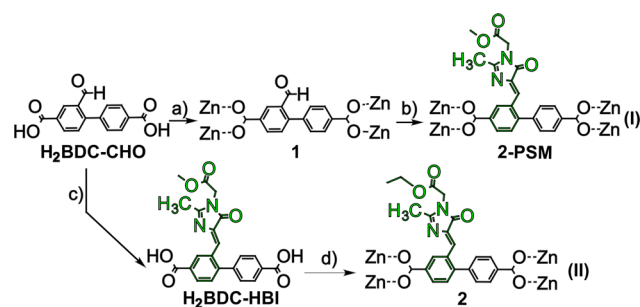
[a]Synthetic routes for H$_2$BDC−HBI immobilization and preparation of **2-PSM** (route I) and **2** (route II) using the following reagents and experimental conditions: (a) Zn(NO$_3$)$_2$, DEF/EtOH, 100 °C, 24 h; (b) methyl-2-((1-ethoxyethylidene)amino)acetate, room temperature, 3 days; (c) H$_2$BDC−HBI was synthesized according to Scheme S1; (d) Zn(NO$_3$)$_2$, DEF/EtOH, 100 °C, 24 h.

chromophore, 2-((1-(2-methoxy-2-oxoethyl)-2-methyl-5-oxo-1,5-dihydro-4H-imidazol-4-ylidene)methyl)-[1,1'-biphenyl]-4,4'-dicarboxylic acid (H$_2$BDC−HBI, Scheme 2), was prepared in situ by postsynthetic modification (PSM) of a crystalline scaffold, and (**II**) H$_2$BDC−HBI, prepared using a five-step synthetic procedure, was used as a linker to synthesize a rigid scaffold under solvothermal conditions (Schemes 2 and S1 and Figure S1, see the Supporting Information (SI) for more details). In the case of procedure **I**, the choice of the parent scaffold was mainly dictated by three criteria: (i) an appropriate pore aperture, which could accommodate the prepared in situ linker, (ii) structural scaffold stability to undergo PSM,[18] and (iii) presence of the reactive group, which could be used to install the HBI-based chromophore. The selected scaffold Zn$_4$O(BDC−CHO)$_3$[26] (**1**, [BDC−CHO]$^{2−}$ = 2-formyl-biphenyl-4,4'-dicarboxylate) possesses a porous structure[26] consisting of Zn$_4$O-(O$_2$C−)$_6$[27] secondary building units as shown in Figures S2 and S3. Furthermore, the framework linker contains a reactive aldehyde group that could be utilized for in situ chromophore formation (Scheme 2). Thus, **1** satisfies all three required criteria (vide supra). In approach **I**, the 1,3-dipolar cyclization reaction with methyl-2-((1-ethoxyethylidene)amino)acetate was utilized for in situ modification of the reactive −CHO group in **1** and therefore conversion of the parent [BDC−CHO]$^{2−}$ to the desired [BDC−HBI]$^{2−}$, as shown in Scheme 2. Approach **II** was based on an initially prepared H$_2$BDC−HBI ligand (Scheme S1),

which underwent solvothermal synthesis with Zn(NO$_3$)$_2$·6H$_2$O at 100 °C for 24 h.

For the comprehensive characterization of the synthesized scaffolds, we employed a combination of X-ray crystallography, thermogravimetric and elemental analyses, infrared spectroscopy, mass spectrometry, and solid-state and solution NMR spectroscopy (including 2D ^{1}H{^{13}C} heteronuclear multiple-bond correlation (HMBC), ^{1}H{^{13}C} heteronuclear single-quantum correlation (HSQC), ^{13}C CP-MAS, and ^{2}H NMR spectroscopies, Figures 1 and S3−S11). As a result, we found that
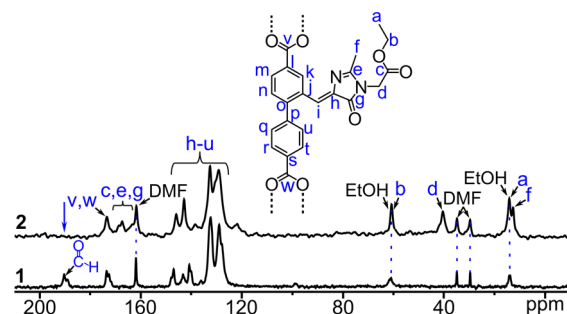
Figure 1. ^{13}C CP-MAS NMR spectra of **1** (bottom) and **2** (top). The blue arrow indicates absence of the peak corresponding to the −CHO group in **2**.

PSM of **1** (approach **I**) occurred through a single-crystal to single-crystal transformation and resulted in preparation of Zn$_4$O(BDC−CHO)$_{1.1}$(BDC−HBI)$_{1.9}$ (**2-PSM**). Notably, the observed degree of [BDC−CHO]$^{2−}$ → [BDC−HBI]$^{2−}$ conversion (64%) was consistent with the literature data (60%) reported for preparation of 2,4-dinitrophenylhydrazine-containing linker using **1** as a postsynthetically modified scaffold.[26] The solvothermal synthesis (**II**) resulted in formation of Zn$_4$O(BDC−HBI')$_3$ (**2**, [BDC−HBI']$^{2−}$ = 2-((1-(2-ethoxy-2-oxoethyl)-2-methyl-5-oxo-1,5-dihydro-4H-imidazol-4-ylidene)methyl)-[1,1'-biphenyl]-4,4'-dicarboxylate, Scheme 2). Combination of solution (1D ^{1}H and ^{13}C, 2D ^{1}H{^{13}C} HMBC, ^{1}H{^{13}C} HSQC) and solid-state ^{13}C CP-MAS NMR spectroscopies revealed that formation of **2** was accompanied by a transesterification reaction, which occurred due to the presence of ethanol in the reaction media (i.e., −OCH$_3$ → −OCH$_2$CH$_3$ conversion, Scheme 2 and Figures 1 and S7−S9). As expected from resemblance of synthetic conditions and linker molecular structures,[27] **1**, **2**, and **2-PSM** (Scheme 2) scaffolds possess the same structures as corroborated by powder X-ray diffraction (PXRD) analysis (Figure S11). Both PXRD studies and single-crystal X-ray analysis demonstrated that integrity of **1** was preserved after the PSM procedure (Figure S11 and Table S1).

Photophysical properties of prepared **2-PSM** and **2** were studied by diffuse reflectance, fluorescence, and time-resolved photoluminescence (PL) spectroscopies. Both diffuse reflectance and fluorescence spectra of **2-PSM** and **2** clearly indicated a bathochromic shift in the absorption and emission profiles compared to parent **1** (Figure 2). The observed shift could be attributed to the extended structure of [BDC−HBI']$^{2−}$ compared to [BDC−CHO]$^{2−}$. As shown in Figure 2, the PL maximum of **2** is red-shifted by 76 nm. Remarkably, the emission maximum of **2** (516 nm) is comparable with the 508−511 nm PL maxima observed in the fluorescence spectra of the natural GFP and its mutants.[28] As expected, the PL profile of **2-PSM** contained two emission maxima corresponding to the [BDC−CHO]$^{2−}$ and [BDC−HBI]$^{2−}$ linkers (Figure S12). Notably, the
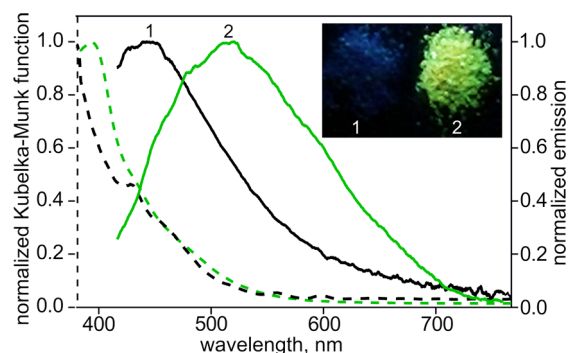
Figure 2. Normalized diffuse reflectance (- - -) and emission (———) spectra of **1** (black) and **2** (green). The inset shows a photograph of **1** and **2** at λ_{ex} = 365 nm.

PL studies of the H$_2$BDC−HBI ligand in solution indicated a 90 nm hypsochromic shift of the emission maximum in comparison with **2**, and the PL quantum efficiency of H$_2$BDC−HBI in tetrahydrofuran (10^{-5} M) was found to be ≤1%. The time-resolved PL studies revealed that the fluorescence decay of **2-PSM** (λ_{ex} = 360 nm) is located between the decay curves of **1** and **2** (Figure S13). This fact is consistent with the acquired emission data (vide supra) and is also in agreement with the presence of two types of ligands contributing to the fluorescence decay profile of **2-PSM**. Analysis of the obtained curves with a reconvolution fit supported triexponential decays for the prepared scaffolds (Figure S13). The intensity-weighted average lifetimes were found to be 4.23, 1.91, and 1.59 ns for **1**, **2-PSM**, and **2**, respectively (see the SI for more details). The determined average lifetimes for **2** and **2-PSM** are shorter than that of GFP (3.03 ns); however, the **2-PSM** lifetime, 1.91 ns, is comparable with those observed for GFP mutants (1.88−1.94 ns).[29] Thus, on the basis of the PL studies, we can conclude that the engineered scaffolds **2** and **2-PSM** mimic the GFP β-barrel behavior by maintaining the emission of an HBI-based chromophore and possessing PL maxima typical for natural GFP-based systems.

As previously demonstrated for GFP-related systems, activation of low-energy vibrational modes in HBI-based molecules could lead to almost complete quenching of chromophore emission.[8,30] For instance, denaturation of GFP resulted in a decrease of PL response by four-orders of magnitude.[11] Therefore, activation of these modes leads to fast nonradiative decay of the excited state, which is restricted by chromophore−β-barrel interactions. To study the effect of the developed rigid scaffold on the chromophore dynamics, solid-state quadrupolar spin−echo ^{2}H NMR and ^{13}C CP-MAS NMR spectroscopic techniques[31−35] coupled with density functional theory (DFT) calculations were employed. For ^{2}H NMR investigations, we attempted to introduce a deuterated tag, −CD$_3$, into the prepared scaffolds through (i) the PSM of **1** by analogy with nondeuterated **2-PSM** (Schemes 2 and S2) and (ii) preparation of deuterated linker, H$_2$BDC−HBI-d_3, following solvothermal synthesis. In both cases, methyl-2-((1-ethoxyethylidene)amino)acetate-d_3 prepared directly from deuterated acetonitrile was used as a source for the −CD$_3$ group (Scheme S2). To implement the solvothermal approach, we synthesized H$_2$BDC−HBI-d_3. However, because of proton exchange during framework solvothermal synthesis, there was no signal corresponding to the deuterated ligand. In contrast, the PSM procedure resulted in the successful formation of **2-PSM-**d_3, ^{2}H NMR spectra of which revealed a superposition of the

sharp isotropic peak and Pake pattern with quadrupolar coupling C_Q = 52 Hz (Figure 3). According to the control experiment
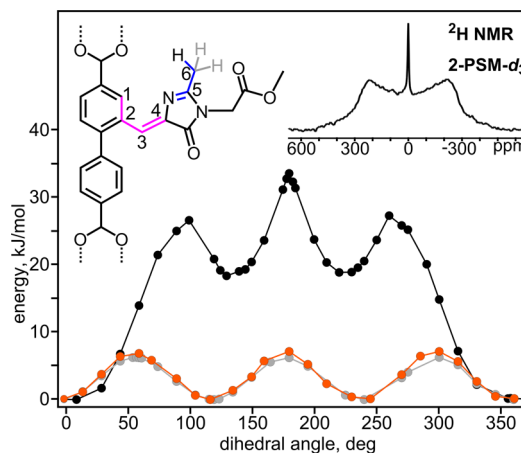

Figure 3. PESs for CH$_3$ group and C$_2$−C$_3$ single bond dynamics. The black solid line indicates the PES constructed for C$_2$−C$_3$ flip. The PESs for the flipping of CH$_3$ group in the confined and unbound chromophores are depicted by gray and orange solid lines, respectively. The carbon atoms define dihedral angles used to model the PESs for motion of the methyl group and around the single bond are depicted by blue and pink colors, respectively. The inset shows the quadrupolar spin−echo ^{2}H NMR spectrum recorded for **2-PSM-**d_3.

performed for nondeuterated **1**, we attributed the isotropic peak to interstitial mobile solvent molecules (Figure S15). This fact is consistent with the previously reported fast dynamics observed for solvent molecules trapped inside porous frameworks.[34] We attributed the origin of the Pake pattern to flipping of the −CD$_3$ group with frequencies less than 10^4 Hz, the slow dynamics of which could be explained by restrictions imposed by the presence of solvent molecules inside the porous framework. To estimate the activation barrier (E_a), we modeled the potential energy surfaces (PESs) of unbound versus restricted H$_2$BDC−HBI. For this purpose, four PESs were constructed to model the −CH$_3$ group dynamics and single bond C$_2$−C$_3$ motions by varying the C$_1$−C$_2$−C$_3$=C$_4$ and N=C$_5$−C$_6$−H dihedral angles, respectively (Figure 3). As shown in Figure 3, the activation barriers for methyl group hopping in the confined and unrestricted chromophores are very similar, 6−7 kJ/mol. Notably, the estimated E_a values for the methyl group dynamics are comparable with those observed in some natural proteins.[36] As expected, in the case of the C$_2$−C$_3$ bond flip, E_a values were significantly higher. For instance, we found that the E_a for the unrestricted chromophore is 33 kJ/mol. For the coordinatively trapped ligand, a flip around this single bond is sterically hindered and could occur only in a limited angle range (Figure S16). As shown in Figure S17, the coordinatively trapped chromophores could not, for instance, accommodate a 180°-conformation without scaffold/ligand decomposition. In contrast, to the immobilized chromophore, the steric repulsion maximum could easily be avoided in the unbound H$_2$BDC−HBI due to the possibility of conformational deviation as shown in Figure S17. Thus, the obtained results clearly indicate that the prepared scaffolds have an impact on the chromophore molecular dynamics and could be utilized to hinder the chromophore motions leading to suppression of low-energy excited-state nonradiative pathways.

The foregoing results demonstrate that the engineered frameworks can serve as GFP β-barrel mimics toward chromophores with a benzylidene imidazolinone core. Moreover, the coordinatively trapped HBI-based fluorophores exhibit similar photophysical properties as natural GFP-based systems. For instance, the observed emission maxima of the engineered porous scaffolds are similar to the natural GFP and its mutants. A combination of both solid-state NMR techniques and DFT calculations revealed that coordinative immobilization of the chromophore inside the porous scaffold affects chromophore dynamics, resulting in the suppression of low-energy vibrational modes and therefore emission preservation. We envision that the approach presented here could foreshadow the use of extended frameworks for control of molecular conformation and rigidity of typically nonemissive synthetic HBI analogues,[7] development of artificial systems mimicking the natural chromophore environment, and design of materials with tunable or enhanced photoluminescence responses.

■ ASSOCIATED CONTENT

Ⓢ Supporting Information

NMR and FTIR spectra, mass-spectrometry data, DFT-calculated molecular conformations and PESs, TGA traces, synthetic details, X-ray structure refinement data, and fluorescence spectra. This material is available free of charge via the Internet at http://pubs.acs.org.

■ AUTHOR INFORMATION

Corresponding Author
*shustova@sc.edu

Notes
The authors declare no competing financial interest.

■ ACKNOWLEDGMENTS

■ REFERENCES

(1) Yuan, W. Z.; Lu, P.; Chen, S.; Lam, J. W. Y.; Wang, Z.; Liu, Y.; Kwok, H. S.; Ma, Y.; Tang, B. Z. *Adv. Mater.* **2010**, *22*, 2159.

(2) Hong, Y.; Lam, J. W. Y.; Tang, B. Z. *Chem. Soc. Rev.* **2011**, *40*, 5361.

(3) Hughs, M.; Jimenez, M.; Khan, S.; Garcia-Garibay, M. A. *J. Org. Chem.* **2013**, *78*, 5293.

(4) Liu, Y.; Tang, Y.; Barashkov, N. N.; Irgibaeva, I. S.; Lam, J. W. Y.; Hu, R.; Birimzhanova, D.; Yu, Y.; Tang, B. Z. *J. Am. Chem. Soc.* **2010**, *132*, 13951.

(5) Zhao, Z.; Chen, S.; Deng, C.; Lam, J. W. Y.; Chan, C. Y. K.; Lu, P.; Wang, Z.; Hu, B.; Chen, X.; Kwok, H. S.; Ma, Y.; Qiu, H.; Tang, B. Z. *J. Mater. Chem.* **2011**, *21*, 10949.

(6) Meech, S. R. *Chem. Soc. Rev.* **2009**, *38*, 2922.

(7) Niwa, H.; Inouye, S.; Hirano, T.; Matsuno, T.; Kojima, S.; Kubota, M.; Ohashi, M.; Tsuji, F. I. *Proc. Natl. Acad. Sci. U.S.A.* **1996**, *93*, 13617.

(8) Tolbert, L. M.; Baldridge, A.; Kowalik, J.; Solntsev, K. M. *Acc. Chem. Res.* **2012**, *45*, 171.

(9) Ward, W. W.; Bokman, S. H. *Biochemistry* **1982**, *21*, 4535.

(10) Baranov, M. S.; Lukyanov, K. A.; Borissova, A. O.; Shamir, J.; Kosenkov, D.; Slipchenko, L. V.; Tolbert, L. M.; Yampolsky, I. V.; Solntsev, K. M. *J. Am. Chem. Soc.* **2012**, *134*, 6025.

(11) Baldridge, A.; Samanta, S. R.; Jayaraj, N.; Ramamurthy, V.; Tolbert, L. M. *J. Am. Chem. Soc.* **2011**, *133*, 712.

(12) Baranov, M. S.; Solntsev, K. M.; Lukyanov, K. A.; Yampolsky, I. V. *Chem. Commun.* **2013**, *49*, 5778.

(13) Rafiq, S.; Rajbongshi, B. K.; Nair, N. N.; Sen, P.; Ramanathan, G. *J. Phys. Chem. A* **2011**, *115*, 13733.

(14) Deng, H.; Zhu, Q.; Wang, D.; Tu, C.; Zhu, B.; Zhu, X. *Polym. Chem.* **2012**, *3*, 1975.

(15) Jung, S.; Kim, Y.; Kim, S.-J.; Kwon, T.-H.; Huh, S.; Park, S. *Chem. Commun.* **2011**, *47*, 2904.

(16) Brantley, J. N.; Bailey, C. B.; Cannon, J. R.; Clark, K. A.; Vanden Bout, D. A.; Brodbelt, J. S.; Keatinge-Clay, A. T.; Bielawski, C. W. *Angew. Chem., Int. Ed.* **2014**, *53*, 5088.

(17) Deng, H.; Grunder, S.; Cordova, K. E.; Valente, C.; Furukawa, H.; Hmadeh, M.; Gándara, F.; Whalley, A. C.; Liu, Z.; Asahina, S.; Kazumori, H.; O'Keeffe, M.; Terasaki, O.; Stoddart, J. F.; Yaghi, O. M. *Science* **2012**, *336*, 1018.

(18) Cohen, S. M. *Chem. Rev.* **2012**, *112*, 970.

(19) Chae, H. K.; Siberio-Pérez, D. Y.; Kim, J.; Go, Y.; Eddaoudi, M.; Matzger, A. J.; O'Keeffe, M.; Yaghi, O. M. *Nature* **2004**, *427*, 523.

(20) Farha, O. K.; Yazaydın, A. Ö.; Eryazici, I.; Malliakas, C. D.; Hauser, B. G.; Kanatzidis, M. G.; Nguyen, S. T.; Snurr, R. Q.; Hupp, J. T. *Nat. Chem.* **2010**, *2*, 944.

(21) Furukawa, S.; Reboul, J.; Diring, S.; Sumida, K.; Kitagawa, S. *Chem. Soc. Rev.* **2014**, *43*, 5700.

(22) Lu, W.; Wei, Z.; Gu, Z.-Y.; Liu, T.-F.; Park, J.; Park, J.; Tian, J.; Zhang, M.; Zhang, Q.; Gentle Iii, T.; Bosch, M.; Zhou, H.-C. *Chem. Soc. Rev.* **2014**, *43*, 5561.

(23) Zhang, T.; Lin, W. *Chem. Soc. Rev.* **2014**, *43*, 5982.

(24) Lee, C. Y.; Farha, O. K.; Hong, B. J.; Sarjeant, A. A.; Nguyen, S. T.; Hupp, J. T. *J. Am. Chem. Soc.* **2011**, *133*, 15858.

(25) Williams, D. E.; Rietman, J. A.; Maier, J. M.; Tan, R.; Greytak, A. B.; Smith, M. D.; Krause, J. A.; Shustova, N. B. *J. Am. Chem. Soc.* **2014**, *136*, 11886.

(26) Burrows, A. D.; Frost, C. G.; Mahon, M. F.; Richardson, C. *Angew. Chem., Int. Ed.* **2008**, *47*, 8482.

(27) Eddaoudi, M.; Kim, J.; Rosi, N.; Vodak, D.; Wachter, J.; O'Keeffe, M.; Yaghi, O. M. *Science* **2002**, *295*, 469.

(28) Follenius-Wund, A.; Bourotte, M.; Schmitt, M.; Iyice, F.; Lami, H.; Bourguignon, J.-J.; Haiech, J.; Pigault, C. *Biophys. J.* **2003**, *85*, 1839.

(29) Scruggs, A. W.; Flores, C. L.; Wachter, R.; Woodbury, N. W. *Biochemistry* **2005**, *44*, 13377.

(30) Baldridge, A.; Feng, S.; Chang, Y.-T.; Tolbert, L. M. *ACS Comb. Sci.* **2011**, *13*, 214.

(31) Vogelsberg, C. S.; Bracco, S.; Beretta, M.; Comotti, A.; Sozzani, P.; Garcia-Garibay, M. A. *J. Phys. Chem. B* **2012**, *116*, 1623.

(32) Jiang, X.; Rodríguez-Molina, B.; Nazarian, N.; Garcia-Garibay, M. A. *J. Am. Chem. Soc.* **2014**, *136*, 8871.

(33) Commins, P.; Garcia-Garibay, M. A. *J. Org. Chem.* **2014**, *79*, 1611.

(34) Shustova, N. B.; Ong, T.-C.; Cozzolino, A. F.; Michaelis, V. K.; Griffin, R. G.; Dincă, M. *J. Am. Chem. Soc.* **2012**, *134*, 15061.

(35) Murdock, C. R.; McNutt, N. W.; Keffer, D. J.; Jenkins, D. M. *J. Am. Chem. Soc.* **2014**, *136*, 671.

(36) Struts, A. V.; Salgado, G. F. J.; Martínez-Mayorga, K.; Brown, M. F. *Nat. Struct. Mol. Biol.* **2011**, *18*, 392.